Defects and Disorder: Probing the Surface Chemistry of Heterogenite (CoOOH) by Dissolution Using Hydroquinone and Iminodiacetic Acid

R. Lee Penn,*,† Alan T. Stone,‡ and David R. Veblen†

Department of Earth and Planetary Sciences and Department of Geography and Environmental Engineering, Johns Hopkins University, Baltimore, Maryland 21218
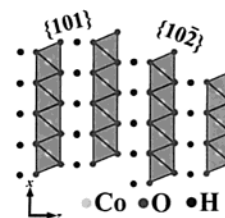
Received: October 27, 2000; In Final Form: March 8, 2001

High-resolution transmission electron microscopy (HRTEM) results show a strong crystal-chemical dependence on the mode of dissolution of synthetic heterogenite (CoOOH) particles via ligand-assisted dissolution using iminodiacetic acid (IDA) and reductive dissolution using hydroquinone (H$_2$Q). Dissolution, using H$_2$Q (10 μM to 2 mM) and IDA (10 μM to 2 mM), of synthesized heterogenite particles (37 mg/L) was examined in order to evaluate morphology evolution as a function of dissolution agent concentration. No evidence for redox reactions was observed in experiments using IDA, and no aqueous complexes of Co(II) or Co(III) with H$_2$Q or benzoquinone, the oxidation product of H$_2$Q, in experiments using H$_2$Q were detected. As-synthesized heterogenite particles are micron-size hexagonal plates (aspect ratio, ∼1/30) constructed of crystallographically oriented ∼5 nm primary particles, or they are single ∼21 nm or ∼10 nm unattached heterogenite platelets (aspect ratio, ∼1/7 and ∼1/3, respectively). In experiments using the micron-sized hexagonal plates, two dominant modes of dissolution were observed: nonspecific dissolution that dissolved primary building blocks at all locations equally and pathway specific dissolution that occurred along boundaries of misorientation between primary building blocks. Both mechanisms occurred independent of the dissolution agent used. In comparison, TEM results show that dissolution of the unattached heterogenite particles occurs primarily at the {101} and {10$\bar{2}$}, or "edge," crystal faces and that no significant dissolution occurs at the (001), or "basal," crystal faces. This suggests that the reactive surface area is dominated by edge faces and further suggests that basal faces are essentially nonreactive under these conditions. Finally, dissolution by IDA produced two dissolved isomers, *u-fac* Co[IDA]$_2^-$ and *s-fac* Co[IDA]$_2^-$. Experiments using identical solution conditions show that dissolution of the micron-sized plates favors the production of the *u-fac* isomer while dissolution of the 21 nm particles favors the production of the *s-fac* isomer.

1. Introduction

Dissolution of solid phases at the earth's surface can liberate elemental constituents by processes ranging from the production of aqueous ions and molecular complexes to nanocrystalline particles that can move by colloidal transport. These two end-member processes involve surface and crystal chemistry. Since much of the reactive surface area in Earth's near-surface environments is comprised of nanocrystalline materials (e.g., clays and oxyhydroxides[1]), experiments involving such materials are vital to understanding dissolution and precipitation mechanisms operating at the earth's surface. Coupling high-resolution transmission electron microscopy (HRTEM) with wet chemical methods allows direct comparison of atomic-scale changes in dissolving materials with changes in solution and surface chemistry.

^{60}Co is a radionuclide and an appreciable component in radioactive wastes.[2,3] Co(II) is more soluble than Co(III), and Co(II) complexes are one of the dominant forms of transportable cobalt in the environment. Thus, reductive dissolution of Co(III) sorbed to or precipitated on mineral surfaces in the environment or Co(III)-bearing minerals, such as heterogenite, could result in the enhanced transport of Co. Alternatively, Co(III) solubility can be enhanced by complexation by organic molecules such as carboxylates, iminocarboxylates, or phosphonates.[4] This

* Corresponding author. E-mail: penn@chem. umn.edu. FAX: 410 516 7933.
† Department of Earth and Planetary Sciences.
‡ Department of Geography and Environmental Engineering.

Figure 1. Polyhedral representation of the CoOOH (heterogenite) crystal structure, which consists of layers of edge-sharing Co(III) oxohydroxo octahedra.

work's focus involves dissolution experiments using two different morphologies of heterogenite (CoOOH) particles and two chemically distinct modes of dissolution: reductive dissolution and ligand-assisted dissolution.

Heterogenite has a brucite-like structure constructed of layers of edge-sharing Co(III) oxohydroxo octahedra (Figure 1). This mineral belongs to a class of minerals, the oxyhydroxides, which are important because they comprise a large proportion of reactive surface area in the environment (e.g., as products of biomineralization in soils, as mineral weathering products, and as mineral coatings[5,6]). In addition, the structures of many of the oxyhydroxides are simple and relatively well understood. Although Fe-bearing oxyhydroxides and oxides are certainly more abundant on the earth's surface, many aqueous complexes of iron are too labile to analytically separate and characterize. In comparison, aqueous Co complexes are amenable to analytical characterization because they undergo ligand exchange quite

slowly. Thus, dissolution experiments using a Co-bearing mineral provide a good starting point for probing surface reactivity and structure using wet chemical methods.

A systematic investigation of the variation in surface chemistry with changing functional groups and substitution on the dissolution agent molecule can lead to predictions regarding the more complex chemicals commonly used by plants and other organisms to extract nutrients from soils and rocks.[7] Ligand-assisted dissolution will result in complexed Co in solution or adsorbed to surfaces, while reductive dissolution will result in the production of Co(II) cations, which may be sorbed to surfaces or may react with aqueous species to produce Co(II) complexes. For the interpretation of experimental results to be simplified, a good reductive dissolution agent should not participate in complexation reactions, and a good ligand-assisted dissolution agent should not be redox active.

Reductive dissolution by hydroquinone has been previously studied and shown to reduce Co(III) according to eq 1, where Q refers to benzoquinone and QH_2 refers to hydroquinone[8]

$$2 \, Co(III)OOH(s) + QH_2(aq) + 4H^+(aq) =$$
$$2 \, Co^{2+}(aq) + Q(aq) + 4 \, H_2O \quad (1)$$
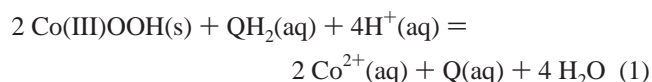
Ligand-assisted dissolution by IDA has been previously studied by McArdell et al.[4] They showed that IDA does not reduce Co(III) and that the stoichiometric ratio of Co:IDA is 1:2, as shown in eq 2

$$Co(III)OOH(s) + 3H^+(aq) + 2IDA^{2-}(aq) =$$
$$[Co(III)IDA_2]^-(aq) + 2H_2O \quad (2)$$
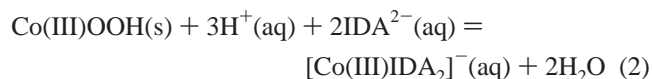
In addition, they showed that different preparations of CoOOH preferentially produce one of two isomers of $[Co(IDA)_2]^-$ (McArdell and Stone, in preparation). This work attempts to draw comparisons between reductive and ligand-assisted dissolution of two different morphologies of heterogenite particles and to link chemical behavior with the detailed microstructure in this model system.

2. Experimental Procedure

All suspensions and solutions were prepared using reagent-grade chemicals and 18 MΩ·cm resistivity water (DDW, Millipore Corp.). Hydroquinone (99+%), *p*-benzoquinone (99+%), and iminodiacetic acid (IDA, 98%) were purchased from Aldrich Chemical Co., Inc. All chemicals were used without further purification. Glassware and plasticware were soaked in 5 M HNO_3, rinsed several times with distilled, deionized water, and rinsed several times with DDW prior to use.

Preparation of Synthetic Heterogenite (CoOOH) Particles. Two batches of heterogenite particles were prepared using $Co(II)Cl_2 \cdot 6H_2O$ as the precursor at millimolar concentrations. An oxidant, either hydrogen peroxide or sodium hypochlorite solution, was added during or after precipitation using sodium hydroxide solution. In all cases, electron diffraction and X-ray diffraction results confirmed the formation of heterogenite. The details of each synthesis follow.

In batch CoOOH-1, particles were prepared using a modified method of Stone and Ulrich,[8] which involved precipitation of Co(II) hydroxide followed by oxidation using hypochlorite solution (VWR Sodium Hypochlorite solution, 6%). A 3000 mL solution of 2.33 mM NaOH (Aldrich) was sparged overnight using Ar and heated to 80 °C using a water bath. In addition, 3000 mL of DDW was sparged overnight using Ar and heated

to 80 °C. A 100 mL 35 mM solution of $CoCl_2 \cdot 6H_2O$ (Baker Analyzed) was prepared and filtered through a 0.2 μm Nuclepore polycarbonate track etch filter and added to the sparging, 80 °C DDW ([Co] ≈ 1.2 mM). Approximately 2 h after these solutions were prepared, the NaOH solution was added to the Co(II) solution using a peristaltic pump, producing a pink-colored precipitate. Delivery of the entire volume of NaOH took 1.25 h. The receiving jug was hand-rocked during the addition. The suspension was pale pink. Eighteen minutes after the base delivery was complete, 1000 mL of a 17.5 mM NaOCl solution was quickly added. The suspension immediately turned brown. Five hours after oxidation, the reaction jug was removed from the hot water bath and placed in a cool water bath.

In batch CoOOH-2, particles were prepared using a modified method of McArdell et al.,[4] which involved precipitation of Co(II) hydroxide followed by oxidation using a hydrogen peroxide solution (containing <1 ppm tin as a stabilizer, EM Science). DDW was sparged overnight using Ar and cooled using an ice–water bath. During the synthesis, suspension and solution temperatures ranged from 4 to 7 °C. Using the sparged and cooled DDW, a 3000 mL solution of 2.92 mM NaOH (Aldrich) and a 100 mL solution of 35.0 mM $CoCl_2 \cdot 6H_2O$ (Baker Analyzed) were prepared. The $CoCl_2$ solution was filtered through a 0.2 μm Nuclepore polycarbonate track etch membrane prior to being added to 2900 mL of the sparged and cooled DDW. Both "final" solutions continued to be sparged until the end of the synthesis. Approximately 1 h after these solutions were prepared, the NaOH solution was added to the pale pink Co solution using a peristaltic pump, producing a pink-colored precipitate. Delivery of the entire volume of NaOH took 1.20 h. The receiving jug was stirred using a Teflon-coated magnetic stir bar during the addition to ensure adequate mixing. One minute after the base delivery was complete, 250 mL of the 35.1 mM hydrogen peroxide solution was quickly added. The suspension immediately turned brownish green. Ten minutes later, an additional 250 mL of 35.1 mM hydrogen peroxide solution was quickly added, and the suspension became browner. After an additional 20 min, the remaining 500 mL of 35.1 mM hydrogen peroxide solution was quickly added. The resulting suspension was dark brown. Approximately 8 h after oxidation, the reaction jug was removed from the ice–water bath and placed in a room-temperature water bath.

Suspension concentration was determined by dissolving the particles using hydrochloric acid followed by flame atomic absorption spectroscopy (AAS) to determine total Co in the resultant solution. The CoOOH-1 and CoOOH-2 suspensions contained 500 and 538 μM Co as heterogenite particles. These results were confirmed in dissolution experiments where all heterogenite added was dissolved. The presence of heterogenite was verified using X-ray diffraction analysis. A small volume of each suspension was centrifuged and resuspended using purified water in order to prepare samples for TEM examination and particle size characterization. A small volume of the CoOOH-1 suspension was removed and quenched to room-temperature 5 min after the oxidation step was completed. On the basis of TEM examination, there were no noticeable differences between aged and nonaged samples.

Dissolution Experiments. Suspensions of constant Co concentration (0.4 mmol/L as heterogenite particles) were prepared using a constant concentration of acetate buffer (10 mM, pH 4.6) and varying concentrations of hydroquinone or IDA. Suspensions were allowed to react, with constant shaking, from 10.5 h to 20 days at room temperature. In suspensions containing hydroquinone, suspension pH consistently rose approximately

1/10 of a pH unit after equilibration (12−24 h, from an initial pH ranging from 4.5 to 4.6 to a final pH ranging from 4.6 to 4.7). In suspensions containing IDA, suspension pH was stable throughout the course of the experiments (up to 20 days). Suspensions were filtered using 0.1 μm Nuclepore track etch membranes. By visual inspection, less material was retained on filter membranes as dissolution agent concentration increased. Resulting supernatant solutions were clear and colorless in all cases. At higher concentrations (>0.20 mM hydroquinone or >1mM IDA), no solid was apparent on the filter membranes. To prevent precipitation of acetate salts in preparing TEM specimens, we rinsed filter membranes by passing 5−10 mL DDW through each. Rinsed membranes were placed in 1.5 mL Eppendorf vials with ∼1 mL DDW. Following sonication and vigorous shaking, one drop of each resulting suspension was placed on holey carbon-coated TEM grids and allowed to dry.

For suspensions containing hydroquinone, each filtrate was analyzed for hydroquinone, benzoquinone, and total dissolved Co. For suspensions containing IDA, each filtrate was analyzed for $Co(IDA)_2$ complexes, free IDA, and total dissolved Co. Hydroquinone and benzoquinone concentrations were determined using a reverse-phase HPLC (Waters Corp.) equipped with a variable wavelength UV detector, a μBondapak C18 guard column, a μBondapak C18 3.9 × 300 mm column with a 10 μm packing size, and an autosampler. The eluent was pumped using two pumps and total flow adjusted to deliver ∼17% methanol (HPLC grade) and ∼83% 10 mM acetic acid at a total flow rate of 1 mL/min. Each injection volume was 50 μL of filtrate (dilution ranging from a factor of 1 to a factor of 3). The concentrations of free IDA and $Co(IDA)_2$ complexes were determined using a Quanta 4000E capillary electrophoresis instrument (Waters Corp.) in capillary zone electrophoresis mode using the method reported by Bürgisser and Stone.[9] A bare fused silica capillary with a 75 μm inner diameter and 60 cm length (to the detector) was used. The electrolyte solution was a 25 mM phosphate buffer (pH 7) and 0.5 mM tetradecyl trimethylammonium bromide (TTAB, Aldrich). TTAB sorbs to the reactive silanol sites of the silica capillary and thus prevents sorption of analyte metal complexes and free IDA.[4] The total dissolved Co was determined using atomic absorption spectroscopy (AAS).

Electron Microscopy. All materials were examined using a Philips CM300FEG transmission electron microscope (TEM) equipped with a Gatan Imaging Filter (GIF) for energy-filtered imaging. All TEM images were collected using a Gatan CCD and Digital Micrograph software. Zero-loss TEM images in this work are formed using an energy-filtering technique that excludes electrons that have undergone significant energy losses due to inelastic scattering events (e.g., inner-shell ionization and plasmon interactions). The electron beam passes through a magnetic prism, a part of the GIF, and the electron beam is spread as a function of kinetic energy. By using an energy window of 10 eV centered about the accelerating voltage of the microscope, only low-loss (e.g., phonon scattering events) and zero-loss (elastic scattering events) are included in a zero-loss image. The exclusion of higher-loss electrons improves image resolution and contrast.[10] Each sample was prepared by first diluting each suspension with DDW and then placing one drop of each resulting suspension on holey carbon TEM grids.

3. Results and Discussion

As-Synthesized Particle Characterization. CoOOH-1 particles are hexagonal plates that are comprised of networked and oriented ∼3 nm heterogenite nanocrystals, hereafter referred to
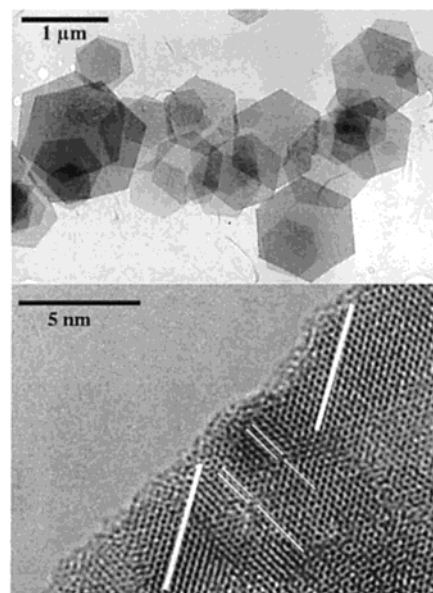

Figure 2. Upper image is a TEM micrograph showing the overall morphology of the plates (CoOOH-1). The lower image shows a zero-loss HRTEM image. The heavy white lines serve to highlight low-angle tilt boundaries between building block crystallites, and the narrow white lines highlight the presence of edge dislocations.

as building block crystallites. The average plate width is 0.7 μm, and the average aspect ratio is ∼1/30. Figure 2 (upper) is a zero-loss HRTEM micrograph showing the overall morphology of the plates. The lower image shows a high-resolution zero-loss image that highlights the high degree of orientation between constituent building block crystallites. The boundaries between perfectly aligned building blocks are crystallographically coherent. In addition, the particles contain numerous low-angle tilt boundaries between building block crystallites that result in the incorporation of dislocations, highlighted by white lines in the lower image of Figure 2. This is most likely due to atomic-scale roughness, such as surface steps, of the primary particle surfaces, as discussed in Penn and Banfield's work involving anatase (TiO_2).[11] Misoriented boundaries are observed to span as many as tens of assembled building block crystallites, resulting in intermediate-scale interfaces between regions of perfect internal orientation.

The detailed arrangement of individual building blocks is difficult to assess, since TEM images are formed by transmission of an electron beam through the entire thickness of the plate. However, the large aspect ratio of these micron-sized plates suggests that assembly occurs primarily near or across edge-type surfaces rather than basal-type surfaces (Figure 3). In discussing assembly morphology, the attachment vector is defined as the direction perpendicular to the interface between building block crystallites. If attachment occurs predominantly across edge-type surfaces, the morphology is expected to expand normal to those surfaces, producing thin and wide plate morphologies. If, on the other hand, particles attach across basal-type surfaces, the morphology is expected to extend perpendicular to (001), producing narrow needlelike morphologies. If the probability of attachment across all of the crystal faces were similar, then a morphology that mirrors the building block morphology would be expected. In the case of CoOOH-1, it is proposed that the predominant attachment vectors are contained within (001), since the general morphology is a thin hexagonally shaped plate.

CoOOH-2 particles are crystallites that, on average, are ∼21 nm across and ∼3.5 nm thick. Average particle dimensions were

Surface Chemistry of Heterogenite (CoOOH)

J. Phys. Chem. B, Vol. 105, No. 20, 2001 **4693**
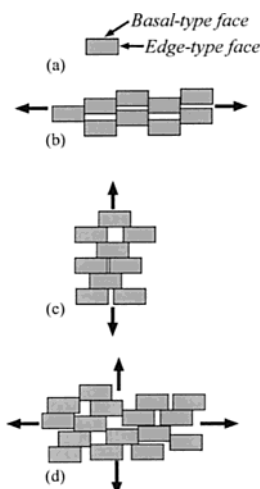
Figure 3. Two-dimensional schematic diagrams of possible arrangements of rectangular building block particles (a). In the discussion of assembly morphology, the attachment vector is defined as the direction perpendicular to the interface between building block crystallites. If assembly occurs predominantly across edge-type surfaces, as in panel b, the assembly expands normal to the edge-type surfaces. If particles assemble across basal-type surfaces, as in panel c, the assembly expands normal to the basal-type surfaces. If the probability of assembly across the edge-type and basal-type faces are similar, as in panel d, then a morphology that resembles the building block morphology is expected.
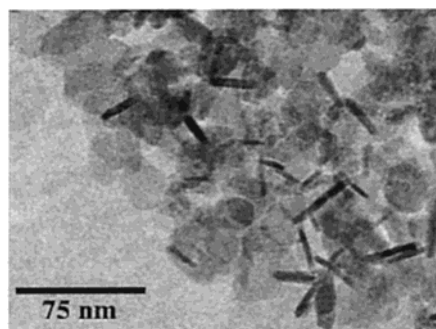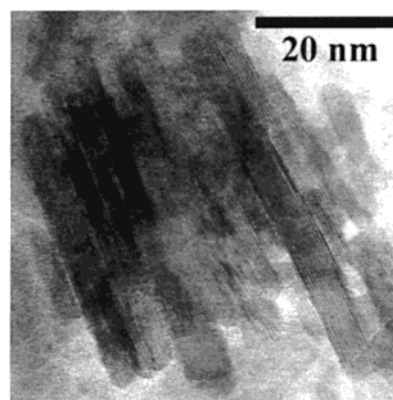

Figure 4. Zero-loss TEM image of CoOOH-2 particles. The crystallites are, on average, ∼21 nm across and ∼3.5 nm thick and generally bounded by {101}, {10$\bar{2}$}, and (001).

determined by measuring the width and thickness of several hundred particles from TEM images. The crystallites (Figure 4) are approximately bounded by {101}, {10$\bar{2}$}, and (001). For the purposes of this work, we have generalized the morphology to consist of two types of crystal surface, edge-type, {101} and {10$\bar{2}$}, and basal-type, (001). In general, no assembly morphology is observed. However, oriented aggregation between several particles is occasionally observed. When such attachment occurs, it is across the basal-type faces, resulting in "books" of heterogenite particles (Figure 5). Most commonly, however, aggregates consist of randomly oriented platelets.

High-resolution TEM reveals an additional difference between CoOOH-1 and CoOOH-2. CoOOH-2 particles contain a high degree of stacking disorder. Figure 6 shows a high-resolution TEM micrograph of a CoOOH-2 particle. The black inset is a Fourier transform of the image, and the streaking in this pattern, specifically in the 10l rows, indicates a high degree of disorder in the stacking of the brucite-like sheets of Co−O octahedra. Such evidence of disorder is not observed for CoOOH-1 particles.

Comparing the structure of Co(II) hydroxide[12] with that of heterogenite reveals a fundamental difference in stacking of the brucite-like sheets of Co octahedra (Figures 1 and 7). In both

Figure 5. Zero-loss HRTEM image of CoOOH-2 particles that have aggregated across basal-type surfaces, resulting in the formation of "books" of particles.
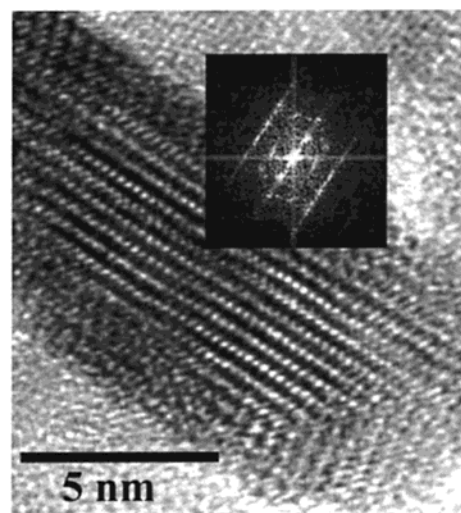
Figure 6. Zero-loss HRTEM micrograph of a CoOOH-2 particle. The black inset is a Fourier transform of the image, and the streaking in this pattern, specifically in the 10l rows, indicates a high degree of disorder in the stacking of the brucite-like sheets of Co−O octahedra.
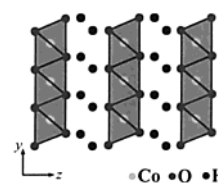

Figure 7. Polyhderal representation of the crystal structure of Co(OH)$_2$, which consists of layers of edge-sharing Co(II) hydroxo octahedra.

cases, the angle between the **a**- and **c**-axes is 90°. However, while the stacking vector and **c**-axis of CO(OH)$_2$ are parallel, projecting a line through the Co cations of neighboring sheets in heterogenite reveals a stacking vector that is inclined by 10.5° with respect to the **c**-axis. When Co(OH)$_2$ is oxidized to form heterogenite, the structure must shear to accommodate the accompanying loss of interlayer protons (one proton is lost per Co cation oxidized). We propose that when peroxide is used as the oxidizing agent, oxidation may occur so rapidly that shearing is not homogeneous, producing disordered stacking of the brucite-like layers (Figure 8). The reaction of peroxide with the suspension of Co(OH)$_2$ is comparatively violent, producing immediate and significant effusion of gas. The color change associated with this transformation is immediately observed upon each addition of peroxide solution. When hypochlorite is used, oxidation is not violent although the color change is rapid.

**TABLE 1: Dimensions of CoOOH-2 Particles before and after Dissolution Using hydroquinone (150 μM and pH 4.6)**

% dissolution	width (nm)	number of particles measured	thickness (nm)	number of particles measured
0	21 (SD 8.6)	402	3.5 (SD 0.9)	123
75	13 (SD 8.7)	344	3.7 (SD 1.0)	116
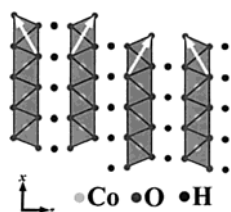
Figure 8. Polyhedral representation of disordered CoOOH. The disorder involves the incorporation of alternating octahedral tilts, denoted by the white arrows. In perfectly ordered heterogenite, the octahedral tilts are all parallel.
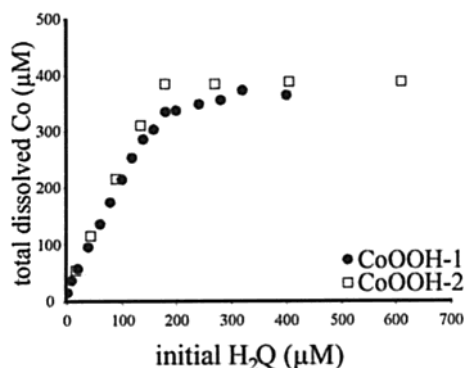
Figure 9. Total dissolved Co vs initial hydroquinone (H$_2$Q) concentration for dissolution experiments using CoOOH-1 and CoOOH-2 particles. All suspensions contained a total Co concentration of 400 μM, added as CoOOH-1 or CoOOH-2 particles, and 10 mM acetate in order to maintain pH near 4.6. The total reaction time was 12 h.

That no evidence for stacking disorder in material oxidized by hypochlorite is observed suggests that the shearing upon oxidation by hypochlorite occurs homogeneously in the transformation from Co(OH)$_2$ to heterogenite.

Reductive Dissolution. The total dissolved Co and ending Q concentration versus initial H$_2$Q concentration, which ranged from 0 to 400 μM, are plotted in Figure 9. The linear relationship between total Q and total dissolved Co is consistent with the reaction stoichiometry predicted in which two Co(III) cations are reduced per H$_2$Q, as in eq 1. This was confirmed by a 1:1 ratio of ending Q, as determined by HPLC, to initial H$_2$Q concentration. These measurements reflect solution chemistry after 12 h of equilibration time, and the slightly rounded shape of the curves for experiments using CoOOH-1 particles indicate that the reaction has not gone to completion. Thus, we conclude this reaction is somewhat slower for these particles. Equilibration of H$_2$Q solutions, without added heterogenite particles, showed no measurable oxidation of H$_2$Q to Q over 12 days time. Mass balance confirms that no sorption of dissolved Co to particle surfaces occurs.

HRTEM examination of post-dissolution CoOOH-1 particles reveals two primary modes of dissolution.[13] In the first case, dissolution appears to occur over the entire surface of the plate (Figure 10). As dissolution progresses, morphologies are increasingly weblike but retain the overall hexagonal-plate shape of the predissolution material. In the second case, dissolution occurs preferentially along boundaries of misorientation between primary building block particles, resulting in the formation of holes and channels (Figure 11). No dependence upon dissolution
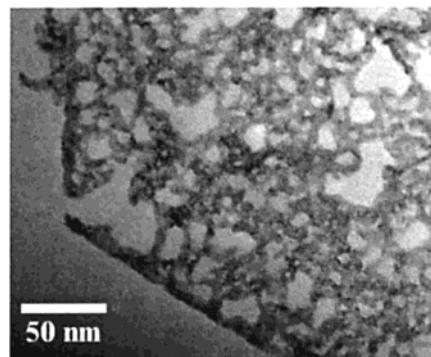
Figure 10. Zero-loss TEM image of a CoOOH-1 particle after partial dissolution by hydroquinone (100 μM) at pH $\sim$4.6 (set by 10 mM acetate buffer). Dissolution occurred over the entire surface of the particle; no pathways of preferential dissolution were observed in this particle.
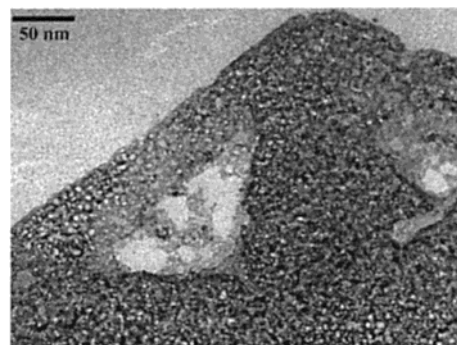
Figure 11. Zero-loss TEM image of a CoOOH-1 particle after partial dissolution by hydroquinone (100 μM) at pH $\sim$4.6 (set by 10 mM acetate buffer). Dissolution occurs preferentially along boundaries of misorientation between primary building block particles, resulting in the formation of holes and channels.

agent is observed. Rather, the degree of match or mismatch between the primary $\sim$5 nm particles controls the way in which CoOOH-1 particles dissolve. Dissolution over the entire surface occurs for particles not containing boundaries of misorientation, and dissolution creating channels and holes occurs in particles containing boundaries of misorientation.

Dimensional measurements of pre- and post-dissolution CoOOH-2 particles shows that dissolution occurs mainly at the edge-type faces (Table 1). The average thickness of platelets does not significantly change while the width of the platelets decreases. This result suggests that the reaction occurs predominantly at the edge-type surface. However, it is important to consider the possibility of electron transfer from the site at which oxidation of hydroquinone occurs to a neighboring Co cation. Thus, the Co(III) cation involved in the oxidation of hydroquinone may not become the Co(II) cation that is released from the structure to the solution.

Despite the incorporation of disorder in CoOOH-2, the structure of individual brucite-like sheets does not change (Figure 12). Edge-type sites are labeled as "2" and "3" and are located on the edge of the brucite-like layer. Edge-type sites are expected to be more reactive than sites contained within the brucite-like layer (e.g., type "1") due to reduced coordinative saturation. In addition, the coordination environment of

Surface Chemistry of Heterogenite (CoOOH)

J. Phys. Chem. B, Vol. 105, No. 20, 2001 **4695**
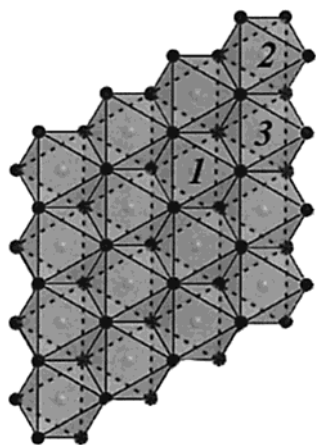
Figure 12. Polyhedral representation of one layer of Co oxohydroxo octahedra. The structure of individual layers does not change with disorder. Edge-type sites are labeled as "2" and "3" and are located on the edge of the layer. Edge-type sites are expected to be more reactive than sites contained within the layer (e.g., type "1") due to reduced coordinative saturation.
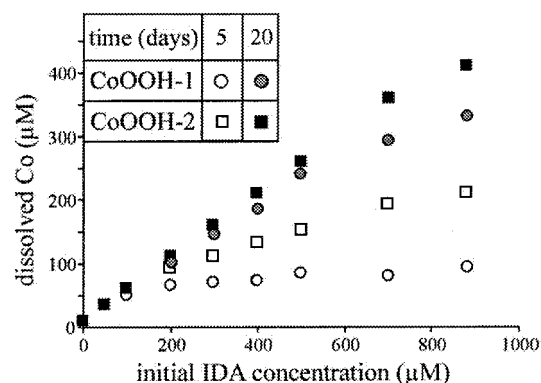

Figure 13. Total dissolved Co vs initial iminodiacetic acid (IDA) for equilibration times of 5 and 20 days (pH ~4.6 using acetate buffer, 400 μM total Co added as CoOOH-1 and CoOOH-2 particles).

Co-cations on the disordered edge-type surfaces is not significantly different when the tilt of the adjacent octahedral layer is coincident or opposite. On the basis of these results, we expect the edge-type surfaces to be most reactive in CoOOH-1 particles. As shown in Figure 3, edge-type surfaces will be exposed regardless of the attachment surface as long as the assembly does not effectively remove all edge-type surfaces.

Ligand-Assisted Dissolution. Total dissolved Co versus starting IDA concentration is shown in Figure 13 for equilibration times of 5 and 20 days in solution (pH ~4.6 using acetate buffer). The linear relationship between total IDA added and total dissolved Co after 21 days is consistent with the reaction stoichiometry of 1 Co cation per 2 IDA molecules, as predicted in eq 2. As in experiments using H_2Q as the dissolution agent, CoOOH-1 dissolves more slowly than CoOOH-2, as reflected in the decreased ratio of total dissolved Co to initial IDA concentration.

HRTEM results reveal morphologies consistent with those observed for dissolution using H_2Q. Both preferential dissolution along misoriented boundaries and dissolution over the entire surface of the micron-sized plates are observed. Again, the mode of dissolution is independent of solution chemistry. Rather, it depends on the occurrence of misoriented boundaries between the primary ~5 nm particles that construct these micron-sized plates. In addition, dimensional measurements of pre- and post-dissolution CoOOH-2 particles reveals dissolution to occur
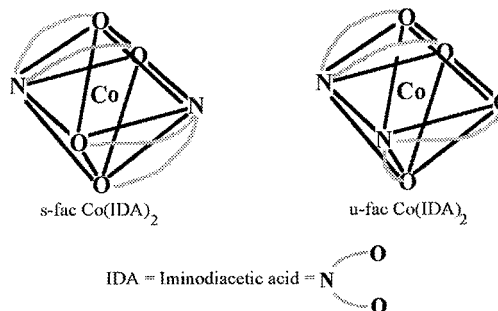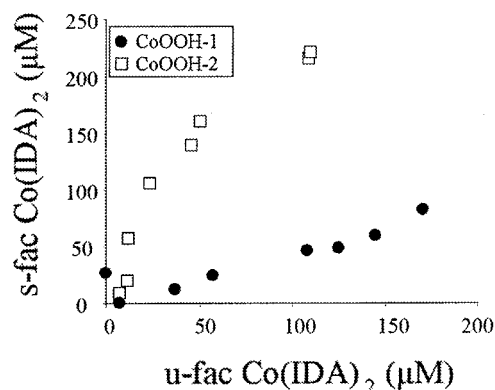

Figure 14. Total concentration of *u-fac* Co(IDA)$_2$ vs *s-fac* Co(IDA)$_2$ after 21 days of reaction. All suspensions contained a total Co concentration of 400 μM, added as CoOOH-1 or CoOOH-2, and 10 mM acetate in order to maintain pH near 4.6. The lower portion of the figure shows schematic representations of the *u-fac* and *s-fac* Co(IDA)$_2$ isomers.

mainly at the edge-type faces, as in experiments using H_2Q as the dissolution agent.

In terms of ligand-assisted dissolution, a sequence involving ligand adsorption, weakening of metal atom−(hydro)oxide bonds, and release of metal ion-ligand complexes is believed to occur.[14] IDA is known to adsorb strongly onto FeOOH (goethite, Whitehead and Stone, in preparation), and strong adsorption onto CoOOH (heterogenite) is also likely. The production of two isomers of Co(IDA)$_2$, *u-fac* and *s-fac*, provides clues regarding the mechanism by which dissolution occurs. The primary difference between these two isomers involves the arrangement of the IDA molecules about the central Co^{3+} cation.[4] Figure 14 shows the structures of the two isomers and the concentration of each isomer produced in dissolution experiments using CoOOH-1 and CoOOH-2. If dissolution were driven simply enhanced solubility due to complexation of Co^{3+} cations by IDA, then no difference between the relative concentrations of each isomer would be expected. Thus, the dissolution mechanism must involve a surface-bound intermediate, the structure of which depends on the detailed arrangement of the particles' surface sites. In addition, the potential complication of interconversion between the *u-fac* and *s-fac* forms of the Co(IDA)$_2$ is avoided by buffering the solution pH using an acetate buffer (solution pH 4.6).[15] Even at circumneutral pH, the interchange between the *u-fac* and *s-fac* forms was observed to be slow, with little change in the ratio of *u-fac* to *s-fac* after several weeks.

The primary structural difference between the two preparations involves the degree of stacking disorder. Comparing Figures 1 and 8 shows the structural difference between perfectly ordered stacking and stacking with a high degree of disorder. While the coordination environments of Co cations at the edge surfaces do not significantly change with stacking disorder, the

4696 *J. Phys. Chem. B, Vol. 105, No. 20, 2001*

Penn et al.
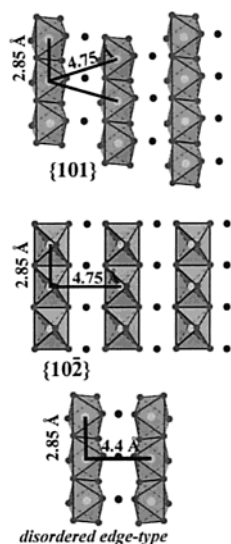
Figure 15. Polyhedral representations of idealized surface layers of CoOOH on the perfectly ordered edge-type surfaces (the {101} and {10$\bar{2}$} faces) and on the disordered edge-type surface. Disorder produces unique strips of surface sites where layers have opposing octahedral tilts. Heavy black lines serve to show the physical spacing between adjacent surface sites.

geometrical arrangement of Co octahedra at the edge surfaces is significantly different. This difference results in the creation of new structural elements, with unique spacings, on the edge-type surfaces. The distance between closest neighbors on perfectly ordered edge-type surfaces is 2.85 and 4.75 Å on {101}, arranged in a rectangular pattern, and 2.85 and 4.8 Å on {10$\bar{2}$}, arranged in a parallelogram pattern with an acute angle of 84° (Figure 15). Stacking disorder serves to create a surface with strips of Co octahedra, arranged in a rectangular pattern, with spacings of ∼4.4 and 2.85 Å. Effectively, the stacking disorder replaces either the {101} or the {10$\bar{2}$} type facets with strips that contain the ∼4.4 and 2.85 Å spacings. The more highly disordered structure favors the production of the *u-fac* isomer of [Co(IDA)$_2$]$^-$, while the more ordered structure favors the production of the *s-fac* isomer. The N-positions are more closely associated in the *u-fac* isomer than in the *s-fac* isomer. It is important to note that the spacing between neighboring Co cations within a single brucite-like layer does not change. It is the spacing between Co cations in adjacent layers that changes with the introduction of stacking disorder.

It is possible to envision a situation where the formation of dissolution products of specific isomeric character involves two adjacent surface complexes. As one [Co^{III}(IDA)]$^+$ moves away from the surface, an adjacent, surface-bound Co$-$IDA may dissociate, producing a free IDA molecule oriented in such a way that a single *u-fac* or *s-fac* [Co(IDA)$_2$]$^-$ complex is produced. Thus, the spacing between Co-sites in adjacent layers may play a key role in the geometry of resulting [Co(IDA)$_2$]$^-$ isomers and provide a route by which specific isomers can be synthesized. Understanding the orientation of surface-sorbed IDA molecules is vital to predicting the dependence of specific surface structural features on the production of chemical species of a particular geometry.

4. Conclusions

The morphology of post-dissolution particles is independent of whether H$_2$Q or IDA is the dissolution agent used. In the case of CoOOH-1 particles, the character of dissolution is observed to depend on the occurrence of misoriented boundaries

between the ∼5 nm building block particles. In the case of CoOOH-2, the evolving aspect ratio as a function of total dissolution of CoOOH-2 particles gives a qualitative measure of the relative reactivities of the edge-type and basal-type faces. These results show that dissolution preferentially occurs at the edge-type faces because the thickness of the particles does not significantly change as dissolution progresses. We can infer that the surface energy, per unit area, is significantly higher for the edge-type faces under these conditions. This result is consistent with Donnay$-$Harker predictions that relate relative surface energy to the interplanar spacings of different crystallographic planes.[16]

Under the conditions employed here, the solubility of CoOOH(s) is exceedingly low. Hence, it is far more likely that dissolution agents react with the CoOOH(s) surface rather than with Co^{3+} aquo and hydroxo species in solution. As far as reductive dissolution is concerned, hydroquinone is an unusually facile reductant. The parent compound, the one-electron oxidation product (semiquinone radical), and two-electron oxidation product (*p*-benzoquinone) experience considerable resonance stabilization, which lowers the activation energy for electron transfer. Reduction of Co^{3+}(aq) and [CoOH]$^{2+}$(aq) by hydroquinone in strongly acidic media has been extensively studied.[17−19] Hydroquinone possesses phenolate groups capable of inner-sphere coordination to Co^{3+}, forming a monodentate complex.[17] Whether the homogeneous phase reaction occurs via an inner-sphere or outer-sphere mechanism has not been completely resolved.[20] The lifetime of the one-electron oxidation product, the semiquinone radical, may also be important. Oxidation of a surface-bound semiquinone radical by a nearest-neighbor Co^{3+} cation versus a Co^{3+} located some distance away may have morphological consequences for the dissolving CoOOH(s) surface.

As far as ligand-assisted dissolution is concerned, earlier work has established that IDA reacts solely through this pathway.[4] IDA possesses three Lewis base groups which are capable of simultaneously coordinating one Co^{3+} center, or bridging between two Co^{3+} ions. As dissolution takes place, complexes with the stoichiometry [Co^{III}(IDA)$_2$]$^-$ fully account for total dissolved cobalt; complexes with the stoichiometry [Co^{III}(IDA)]$^+$ are of negligible importance. Coordination of surface-bound Co^{3+} by one IDA molecule is undoubtedly a prerequisite for dissolution. Coordination of the second IDA molecule either occurs (i) while the Co^{3+} ion is still bound to the surface or (ii) once it has been released into solution as the [Co^{III}(IDA)]$^+$ complex. The *s-fac* geometrical isomer is slightly more thermodynamically favorable than the *u-fac* isomer, and both are considerably more stable than the *mer* isomer.[15] The fact that the relative abundance of the *s-fac* versus the *u-fac* isomer differs for different CoOOH (heterogenite) preparations is strong evidence for coordination of the second IDA molecule prior of release of Co^{3+} from the mineral surface.

These results elucidate the need for detailed structural and microstructural analysis of environmental and synthetic materials involved in chemical reactions. Further experiments require an investigation of the effect of changing the spacing between surface-active groups of dissolution agents and an investigation of steric effects, such as adding a methyl group to the nitrogen of the IDA molecule. Such variation in the molecular structure of dissolution agents can serve as a probe for the mechanism by which these molecules react with mineral surfaces.

Surface Chemistry of Heterogenite (CoOOH)

J. Phys. Chem. B, Vol. 105, No. 20, 2001 **4697**

References and Notes

(1) Hochella, M. F.; Banfield, J. F. Chemical Weathering Rates of Silicate Minerals. In *Reviews in Mineralogy*; White, A. F., Brantley, S. L., Eds.; Mineralogical Society of America: Washington, DC, 1995; Vol. 31, pp 353−406.

(2) Means, J. L.; Crerar, D. A.; Duguid, J. O. *Science* **1978**, *200*, 1477−1481.

(3) Brusseau, M. L.; Zachara, J. M. *Environ. Sci. Technol.* **1993**, *27*, 1937−1939.

(4) McArdell, C. S.; Stone, A. T.; Tian, J. *Environ. Sci. Technol.* **1998**, *32*, 2923−2930.

(5) Banfield, J. F.; Welch, S. A.; Zhang, H. Z.; Ebert, T. T.; Penn, R. L. *Science* **2000**, *289*, 751−754.

(6) Banfield, J. F.; Hamers, R. J. Geomicrobiology: Interactions between Microbes and Minerals. In *Reviews in Mineralogy*; Banfield, J. F., Nealson, K. H., Eds.; Mineralogical Society of America: Washington, DC, 1997; Vol. 35, pp 86−122.

(7) Stone, A. T. Geomicrobiology: Interactions between Microbes and Minerals. In *Reviews in Mineralogyv*; Mineralogical Society of America: Washington, DC, 1997; Vol. 35, pp 309−344.

(8) Stone, A. T.; Ulrich, H. J. *J. Colloid Interface Sci* **1989**, *132*, 509−522.

(9) Burgisser, C. S.; Stone, A. T. *Environ. Sci. Technol.* **1997**, *31*, 2656−2664.

(10) Reimer, L. *Energy-Filtering Transmission Electron Microscopy*; Springer-Verlag: Berline, Heidelberg, 1995; Vol. 71.

(11) Penn, R. L.; Banfield, J. F. *Science* **1999**, *281*, 969−971.

(12) Mockenhaupt, C. H.; Zeiske, T. H.; Lutz, H. D. *J. Mol. Struct.* **1998**, *443*, 191−196.

(13) Penn, R. L.; Stone, A. T.; Veblen, D. R. Preferential Dissolution along Misoriented Boundaries in Heterogenite. In *SYMPOSIUM M: Morphology and Dynamics of Crystal Surfaces in Complex Molecular Systems*, in press.

(14) Furrer, G.; Stumm, W. *Geochim. Cosmochim. Acta* **1986**, *50*, 1847−1860.

(15) Kawaguchi, H.; Ama, T.; Yasui, T. *Bull. Chem. Soc. Jpn.* **1984**, *57*, 2422−2427.

(16) Donnay, J. D.; Harker, D. *Am. Mineral.* **1937**, *22*, 446−467.

(17) Wells, C. F.; Kuritsyn, L. V. *J. Chem. Soc. A* **1969**, 2930−2932.

(18) Pelizzetti, E.; Mentasti, E. *J. Chem. Soc., Dalton Trans.* **1976**, 2222−2225.

(19) Mentasti, E.; Pelizzetti, E.; Giraudi, G. *J. Inorg. Nucl. Chem.* **1976**, *38*, 795−798.

(20) Wells, C. F. *Prog. React. Kinet.* **1995**, *20*, 1−184.